International Journal of Heat and Mass Transfer 53 (2010) 1326–1332

Contents lists available at ScienceDirect

International Journal of Heat and Mass Transfer

journal homepage: www.elsevier.com/locate/ijhmt

Active cooling of a metal hydride system for hydrogen storage

Timothée L. Pourpoint [a], Varsha Velagapudi [b], Issam Mudawar [b], Yuan Zheng [c,*], Timothy S. Fisher [b]

[a] School of Aeronautics and Astronautics, Hydrogen Systems Laboratory, Maurice Zucrow Laboratories – Purdue University, West Lafayette, IN 47907, USA
[b] School of Mechanical Engineering, Hydrogen Systems Laboratory, Maurice Zucrow Laboratories – Purdue University, West Lafayette, IN 47907, USA
[c] Department of Mechanical Engineering, Hydrogen Systems Laboratory, Maurice Zucrow Laboratories – University of Wyoming, Laramie, WY 82071, USA

ARTICLE INFO

Article history:
Received 26 March 2009
Received in revised form 12 November 2009
Accepted 12 November 2009
Available online 4 January 2010

Keywords:
Thermal management
Hydrogen storage
Metal hydride
High pressure
Numerical simulation

ABSTRACT

Reversible high-pressure metal hydrides offer excellent cold start capability and potentially increased hydrogen storage capacity. However, efficient thermal management is a critical issue in this kind of systems. In the present work, hydriding and dehydriding tests have been conducted with 100 g of $Ti_{1.1}MnCr$ metal hydride at pressures up to 330 bar. Thermal characteristics of the $Ti_{1.1}MnCr$ system have been quantified from the experimental data and simulated using a basic numerical model. By varying the coolant flow rates, a hydrogen filling time of 12 min has been achieved.

© 2009 Elsevier Ltd. All rights reserved.

1. Introduction

Alternative energy sources are being sought aggressively to provide solutions to issues related to the environmental impact and cost of fossil fuels. Among the various possible solutions is hydrogen as an energy carrier. Hydrogen when used in fuel cells produces water as the by-product, making it environmentally benign at the point of use. Another advantage of hydrogen is the diversity of primary energy sources that can be used to produce it; including sustainable resources such as wind, hydropower, biomass and solar, as well as existing fossil fuels and nuclear power.

In the automotive industry, many technical challenges must be addressed before a hydrogen-powered vehicle can be realized as an economical and sustainable replacement for existing vehicles. On-board hydrogen storage options include compressed hydrogen, liquid hydrogen, metal hydrides (MHs), chemical hydrides, and cryo-sorbents. Among these methods, metal hydrides offer high volumetric density, comparable to that of liquid hydrogen [1], but most have low gravimetric density [2]. The other disadvantage of metal hydrides is that they release large amounts of heat while hydriding, and the speed of the hydriding process is limited by the hydride's thermal properties and related cooling technologies. Additionally, thermal management of the hydriding process is challenging because of the low thermal conductivity of metal hydrides [3].

The rates of hydrogen absorption and desorption depends on the mass transfer, heat transfer and the reaction kinetics of the metal hydride bed [3,4]. Zhang et al. [5] reviewed the general heat transfer issues involved in the different hydrogen storage methods, and Koh et al. [6] reviewed the kinetics of $LaNi_5$ hydriding kinetics. Most existing literature on metal hydrides has focused on bench-scale studies of reaction kinetics and thermodynamics. However, larger-scale studies are necessary to fully understand the effects of heat and mass transfer on the performance of an on-board hydrogen storage system. At the system scale, issues such as metal hydride kinetics, effective thermal conductivity, and pressurization profiles become paramount to performance.

This work is aimed at testing the hydriding and dehydriding characteristics of a representative high-pressure metal hydride, $Ti_{1.1}MnCr$. Kojima et al. [7] tested the absorption/desorption isotherms of small (10 g) samples of Ti–Cr–Mn–H materials. The metal alloy of $Ti_{1.1}MnCr$ typically exhibits a maximum absorption of 1.8 wt.% of hydrogen in the pressure range of 1 and 330 bar at 296 K, and its heat of formation is −22 kJ/mol H_2 as obtained from the Van't Hoff plots [7,8]. A thermal management system is required to handle the high heat fluxes generated upon absorption in the high-pressure environment.

The present work involves a modular system-scale study of the thermal characteristics of hydrogen absorption/desorption by the material, $Ti_{1.1}MnCr$. Thermal loads are managed by the use of an active coolant flow, and the mass transfer of hydrogen is varied using different pressurization/venting profiles. The effects of these variations on the hydriding and dehydriding temperature profiles of the metal hydride are measured and analyzed.

* Corresponding author. Tel.: +1 307 766 3905; fax: +1 307 766 2695.
E-mail address: yzheng1@uwyo.edu (Y. Zheng).

0017-9310/$ - see front matter © 2009 Elsevier Ltd. All rights reserved.
doi:10.1016/j.ijheatmasstransfer.2009.12.028

Nomenclature

A	heat transfer area, m^2
C	specific heat, kJ/kg K
C_a	hydriding constant, 1/s
E_a	activation energy, kJ/mol H_2
F	fraction of transformation or progress variable
[H]	hydrogen atom concentration, kmol/m^3
h	convection heat transfer coefficient, W/m^2 K
k	hydriding rate or inverse of hydriding time scale, 1/s
L	characteristic conduction length, m
l	characteristic convection length, m
LHV	lower heating value, kJ/kg
[M]	metal atom concentration, kmol/m^3
$\dot{m}'''$	mass flow rate, kg/m^3 s
MH	metal hydride
Nu	Nusselt number
P	filling pressure, bar
Pr	Prandtl number
q'''	volumetric heat release rate, MW/m^3
Re_D	Reynolds number
R_u	universal gas constant, 8.314 J/mol K
T	temperature, K or °C
t	time, s
U	overall heat transfer coefficient, W/m^2 K
WM_H	molecular weight of hydrogen atom, 1 kg/kmol
x	distance, m

Greek symbols

α	thermal diffusivity, m^2/s
δ	wall thickness, m
ε	porosity
ΔH_c	heat of compression, kJ/kg
ΔH_r	heat of reaction (negative for exothermal), kJ/mol H_2
λ	thermal conductivity, W/m K
ρ	density, kg/m^3

Subscripts

eff	effective
eq	equilibrium
Hy	hydriding
m	maximum
p	constant pressure
o	reference state
v	constant volume
∞	ambient

2. Experimental methods

2.1. Metal hydride

The raw material, $Ti_{1.1}CrMn$, is a mixture of three metal powders, titanium, chromium and manganese, mixed in the required atomic ratio of 1.1:1:1. This alloy has to be preprocessed through a two-step activation process to make it reactive and to attain its full capacity of hydrogen absorption of approximately 1.8 wt.%. For this work, a batch of 100 g of metal hydride was activated.

2.2. Lab facility and test module

The Hydrogen Systems Lab at the Purdue University Zucrow Laboratories is comprised of two test cells and a control room for high-pressure testing using hydrogen. It is designed in accordance with NFPA and NASA standards for hydrogen safety. High-pressure reversible metal hydrides are tested in the lab at pressures up to 345 bar. The data acquisition and control systems have been designed to accommodate arbitrary hydrogen pressurization profiles. The facility also has a glove box that has an ultra-high purity argon environment with less than 0.1 ppm of oxygen and less than 0.1 ppm of moisture to store pyrophoric materials such as activated metal hydride powder. The laboratory is also equipped with a closed-loop heat exchanger system with a cooling capacity of 10 kW.

The experimental system consists of a high-pressure hydrogen feed system, pressure vessel assembly, a tube-in-tube heat exchanger for removal of heat from the metal hydride by the coolant flow during absorption, a cooling system to supply coolant flow, data acquisition and instrumentation, and a glove box for material handling. Since high pressures are required for testing the metal hydride, the various components used in the high-pressure systems, namely the pressure vessel, hydrogen feed, supply and vent systems are designed to handle pressures up to approximately 400 bar.

Shown in Fig. 1, the test article is a finned tube-in-tube heat exchanger designed to supply coolant flow in the inner tube and to hold metal hydride powder between the fins. This semi-sectional view outlines the plate fin heat exchanger with an outer tube assembly and a thermocouple probe. The outer tube is a porous tube with a high-temperature filter paper and stainless steel mesh around it. When the pressure vessel is pressurized, the hydrogen fills in all the empty slots and also comes in contact with the metal hydride from all around the tube. As per a scaling analysis of the energy equation [9], a diameter of 51 mm (2″) is used for the outer tube of the heat exchanger. A schematic of the test article and the thermocouple placement is shown in Fig. 2. Only two of the slots, labeled as Slot 1 and Slot 2 in the schematic, are filled with 46.6 g of metal hydride powder each. Probe 1 measures the temperature of the metal hydride and the empty spacing, and probe 2 measures the gas temperature.

2.3. Experimental observation

Various tests were conducted using the 93.2 g of activated metal hydride powder available for the study. Shown in Fig. 3 are the experimental temperatures in the pressure vessel during a representative test. Initially, the coolant flow is set at 0.9 l per minute (lpm) at 4 °C. This cools the metal hydride to 5 °C at $t = 20$ min

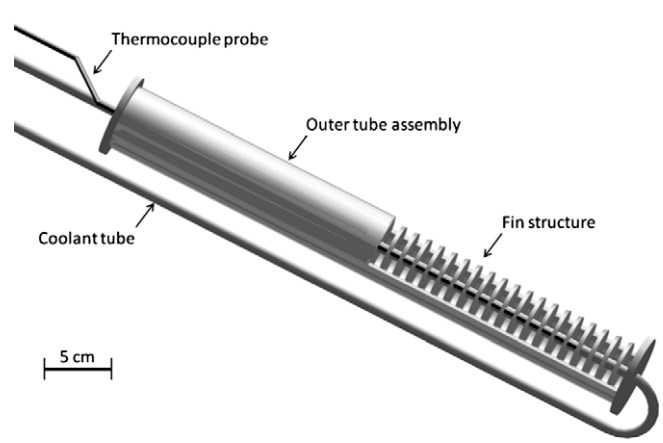

Fig. 1. High-pressure metal hydride test article schematic.

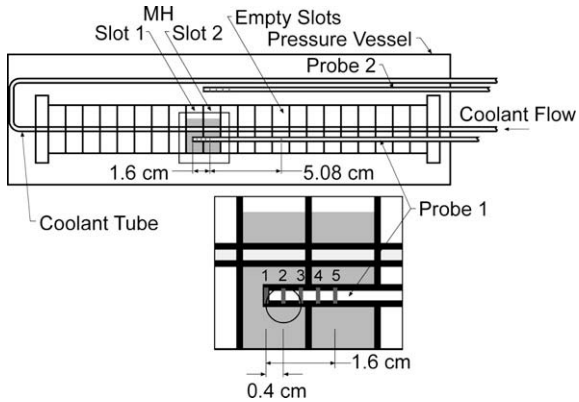

Fig. 2. High-pressure metal hydride test article schematic with temperature probe showing the locations of sensors on the probe.

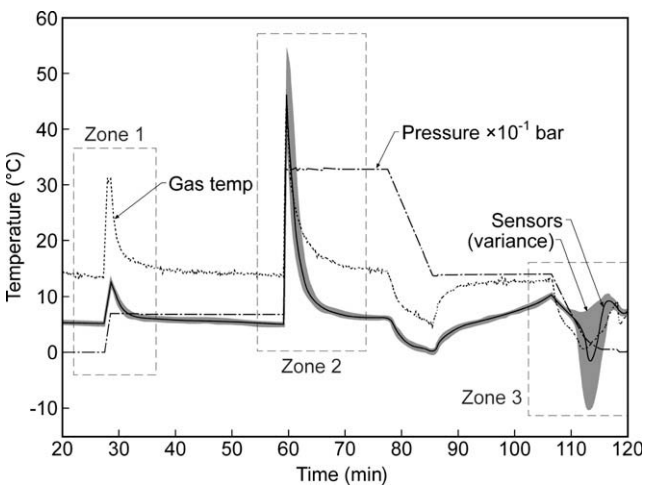

Fig. 3. Temperature and pressure profiles recorded during a typical high-pressure metal hydride test.

while the hydrogen gas is at 14 °C due to a higher ambient temperature. The pressurization profiles are divided into three zones corresponding to three distinct phases. A description of each of the characteristic zone of a typical test is given below.

2.3.1. Zone 1

The pressure vessel is first pressurized from 1 to 68 bar in 60 s with a coolant flow of 0.9 lpm at 4 °C. The gas temperature increases to 31 °C, and the metal hydride temperature increases from 5 to 13 °C. This increase is mainly attributed to compression heating although a small amount of this can be due to the exothermic hydriding reaction.

2.3.2. Zone 2

After allowing the system to cool back down to the starting temperatures, the pressure vessel is pressurized from 68 to 330 bar in 30 s with a coolant flow of 0.9 lpm at 4 °C. The temperatures in the system increases with increasing pressure and then decreases after the pressurization stopped. A maximum temperature of 55 °C is observed in the metal hydride at the locations monitored by sensors 1 and 2. The temperature readings characteristic of Zone 2 are shown in Fig. 4. It is observed that sensors 1 and 2 record nearly the same temperatures, sensors 3 and 4 exhibit similar temperatures, and sensor 5 shows the lowest temperature. Although sensors 2 and 5 are at similar locations in the metal hydride with respect to the fins, their temperature readings differ.

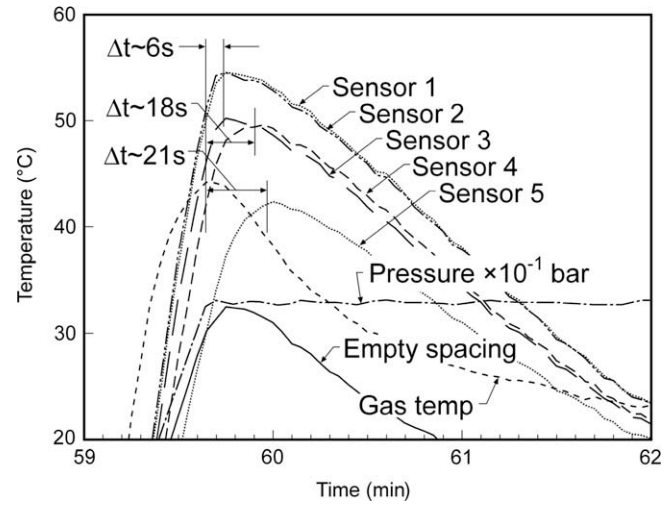

Fig. 4. Peak shift observed in maximum temperatures of different sensors during the pressurization process (Zone 2).

This is attributed to the fin effect of the metal-sheathed thermocouple probe, and this effect is most pronounced at sensor 5. Further, a temporal peak shift of the maximum temperatures is observed in all the tests. The peak shifts for the above typical test are shown on Fig. 4. A shift of up to 21 s in the peak temperatures from the gas temperature to the temperature recorded by sensor 5 was observed in this test. This peak shift is likely due to fin effects caused by the thermocouple probe.

2.3.3. Zone 3

The pressure vessel is vented from 140 to 1 bar by setting the vent regulator upstream of a sonic venturi at 14 bar leading to a constant mass flow rate of 0.5 g/s. A coolant flow of 0.9 lpm at a temperature of 12 °C is used during the venting process. A minimum temperature of −10 °C is observed in sensors 1 and 2. As shown in Fig. 5, the trends observed at various locations in the test article during the venting process are similar to those recorded in the pressurization temperature profiles. Furthermore, as expected, the temperature variations in the empty spacing (gas temperature) is much less than that of the metal hydride.

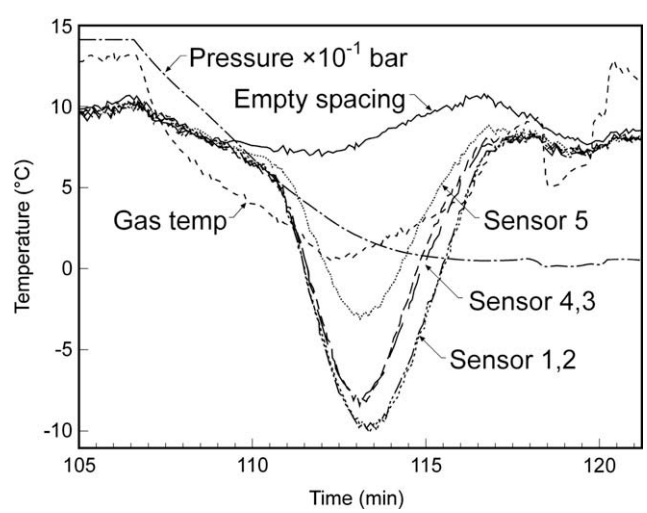

Fig. 5. Temperature and pressure profiles recorded during venting from 140 to 1 bar (Zone 3).

3. Numerical model

The aforementioned experimental results are influenced by a variety of physical phenomena including compression heating, convection between the hydride and filling hydrogen gas, and interfacial heat conduction among particles, hydrogen gas, and solid fins. Numerical modeling has served to aid in the interpretation of the experimental data, and as a result of the physical complexity of the transport processes, we have chosen an effective medium approach for system-level modeling using the best available data and estimates of the thermochemical properties. The following sections describe the major components of the model.

3.1. Kinetics

A complete characterization of the kinetics of $Ti_{1.1}CrMn$ has not been reported in the literature, and hence, the reaction parameters (e.g., activation energy, E_a and Arrhenius constant, C_a) are unknown for this material. The kinetics of $LaNi_5$ on the other hand, have been well documented in previous work [6,10,11]. $LaNi_5$ is an AB_5 type of metal hydride, whereas $Ti_{1.1}MnCr$ is an AB_2 type of metal hydride. Further $LaNi_5$ is a low-pressure metal hydride as compared to $Ti_{1.1}MnCr$. Consequently, compression heating can be ignored in modeling the hydriding process of $LaNi_5$ [12]. However, for $Ti_{1.1}MnCr$, compression heating plays a significant role in the temperature rise. In spite of these differences, the reaction parameters of $LaNi_5$ are reasonable engineering estimates and are used in the present study. Ongoing work at the Hydrogen Systems Lab is aimed at determining key thermal and kinetic properties of $Ti_{1.1}MnCr$ as a function of operating conditions: pressure, temperature, and hydrogen concentration.

The rate-limiting step of $LaNi_5$ kinetics has been suggested to be an interface process, for which the driving force of hydriding is proportional to a function of the pressure (P) of gas and the equilibrium pressure (P_{eq}) of the hydride at that temperature. Naturally, the filling pressure should be kept above the equilibrium pressure (P_{eq}) for the hydriding process to occur. This function, $f(P, P_{eq})$ can take various forms including $\ln(P/P_{eq})$ [9,10] and $(P - P_{eq})$ [13]. In addition, the metal hydride temperature must be kept as low as possible because P_{eq} increases with temperature according to a relationship of the form of Eq. (1) [14].

$$P_{eq} = P_0 \exp\left[\frac{\Delta H_r}{R_u}\left(\frac{1}{T} - \frac{1}{T_0}\right)\right] \tag{1}$$

where P_0, the equilibrium pressure at temperature T_0, and ΔH_r, the heat of reaction, are intrinsic material properties. The heat of reaction, ΔH_r, is a fundamental measure of the metal-hydrogen bond strength and is especially important to thermal management. For a first-order kinetic model, the rate of the overall hydriding process can be described as,

$$\frac{dF}{dt} = k(1 - F) \tag{2}$$

where F, the progress variable, is given by

$$F = \left(\frac{[\mathrm{H}]}{[\mathrm{M}]}\right) \Big/ \left(\frac{[\mathrm{H}]}{[\mathrm{M}]}\right)_{\mathrm{m}} \tag{3}$$

and k, the rate constant, is defined as,

$$k = C_a \exp\left(-\frac{E_a}{R_u T}\right) f(P, P_{eq}) \tag{4}$$

where $f(P, P_{eq})$ is a function of gas and equilibrium pressures such as $\ln(P/P_{eq})$.

3.2. Numerical analysis

For the metal hydride, the energy conservation equation is given by,

$$(\rho C)_{\mathrm{MH}} \frac{\partial T}{\partial t} = -\frac{[\mathrm{H}]_{\mathrm{m}}}{2} \Delta H_r \frac{\partial F}{\partial t} + \lambda_{eff} \nabla^2 T + \dot{q}'''_{\mathrm{MH-H_2}} \tag{5}$$

For the hydrogen phase, the compression heating can be accounted for by making the assumption of negligible hydrogen momentum and negligible spatial variation of pressure in the control volume [15], and hence the energy equation becomes,

$$(\rho C)_{\mathrm{H_2}} \frac{\partial T}{\partial t} = \frac{\partial p}{\partial t} + \lambda_{eff} \nabla^2 T + \dot{q}'''_{\mathrm{H_2-MH}} \tag{6}$$

Making the assumption that the metal hydride and hydrogen temperatures are locally equal, gives $\dot{q}'''_{\mathrm{H_2-MH}} = \dot{q}'''_{\mathrm{MH-H_2}} = 0$. The effective medium approximation then leads to the conservation of energy equation as,

$$(\rho C)_{eff} \frac{\partial T}{\partial t} = -(1 - \varepsilon) \frac{[\mathrm{H}]_{\mathrm{m}}}{2} \Delta H_r \frac{\partial F}{\partial t} + \lambda_{eff} \nabla^2 T + \varepsilon \frac{\partial p}{\partial t} \tag{7}$$

where, $(\rho C)_{eff}$ is an effective volumetric heat capacity that is estimated from an average over a control volume containing the porous metal hydride with hydrogen in the pores.

$$(\rho C)_{eff} = (1 - \varepsilon)(\rho C)_{\mathrm{MH}} + \varepsilon (\rho C_v)_{\mathrm{H_2}} \tag{8}$$

The heat capacity term (left side of Eq. (7)) is defined for the effective medium of the porous metal hydride powder and hydrogen occupying the empty spaces between the particles. The first term on the right side of Eq. (7) is the heat generation term due to hydriding, and the second term is the heat dissipation due to conduction. The specific heat of the TiCrMn metal hydride powder was measured by General Motors Tech Center (Warren, MI) to be approximately 484 J/kg K. The density of the powder was measured to be approximately 2400 kg/m^3 with a porosity of 50%.

There are a number of deviations from the assumed model. An important factor during hydriding/dehydriding cycles is that the volume occupied by the metal hydride powder increases and decreases by up to 30%, causing the particles to break down and become finer [16]. This changes the material properties over the number of cycles. Further, the specific heat and density of hydrogen are functions of temperature. The specific heat of the metal hydride increases with amount of absorption and temperature [17]. These factors are not considered in this work, and an overall $(\rho C)_{eff}$, for the effective media of hydrogen and metal hydride of 1265 kJ/m^3 K is assumed.

The maximum atomic hydrogen content per metal atom, $[\mathrm{H}]_{\mathrm{m}}/[\mathrm{M}]$, of $Ti_{1.1}MnCrH_3$ is 1. The reaction enthalpy, ΔH_r, for the metal hydride is obtained from the slope of the Van't Hoff curve from the pressure-composition-isotherms (PCIs) of the metal hydride, reported in Ref. [7]. The effective thermal conductivity of the metal hydride bed, λ_{eff}, was measured to be 1.45 W/m K at the General Motors Tech Center. Although λ_{eff} varies with temperature, pressure and amount of absorption, it is assumed constant here. The effective thermal conductivity is a function of the reacted fraction, pressure and temperature. It has been observed to decrease with increasing reacted fraction for constant pressure and temperature. For example, the λ_{eff} for a magnesium hydride bed varies from 9 to 4 W/m K from the metallic to the hydrided phase [18]. The effective thermal conductivity increases with a rise in pressure and temperature [18].

The progress variable F is a good indicator of the process, starting from zero at the beginning and tending to unity at the end of hydriding. The hydrogen mass flow rate into a single-port pressure vessel can be related to F as

$$\dot{m}''' = WM_{\mathrm{H}}[\mathrm{H}]_{\mathrm{m}}\frac{dF}{dt} \tag{9}$$

The values of E_a and C_a are taken from Suda et al. [19] on $LaNi_5$ as 20.7 kJ/mol H_2 and 54.7 1/s, respectively.

3.3. Computational geometry and boundary conditions

The test module is a finned assembly that contains the coolant tube with the metal hydride powder contained in the fin slots. Because of geometric symmetry, half the fin slot and half the fin have been included in the numerical simulation shown in Fig. 6. The metal hydride bed is a 2" (50.8 mm) outer diameter, ½" (12.7 mm) long cylinder, and the coolant tube has an outer diameter of 3/8" (9.525 mm). The coolant flow is treated as a convective boundary condition with a heat transfer coefficient and temperature of coolant corresponding to actual test conditions. Shown in Table 1 are the coolant flow values used in the tests with their corresponding Reynolds numbers, maximum observed temperature variations, Nusselts numbers, and heat transfer coefficients. The correlations used to compile the Nusselts numbers are listed in Eqs. (10)–(12).

- Constant wall surface temperature for laminar thermal entry length ($Re_D < 2300$): from Hausen and Kays in Ref. [20]

$$Nu = 3.66 + \left(\frac{0.0668Re_{\mathrm{D}}Pr(D/L)}{1 + 0.04(Re_{\mathrm{D}}PrD/L)^{2-3}}\right) \tag{10}$$

- Fully developed turbulent flow ($0.5 < Pr < 2000$, $3 \times 10^3 < Re_{\mathrm{D}} < 5 \times 10^6$): from Petukhov in Ref. [20]

$$Nu = \left(\frac{(\xi/8)(Re_D - 1000)Pr}{1.07 + 12.7(\xi/8)^{1/2}(Pr^{2/3} - 1)}\right) \tag{11}$$

where

$$\xi = (0.790\ln Re_D - 1.64)^{-2} \tag{12}$$

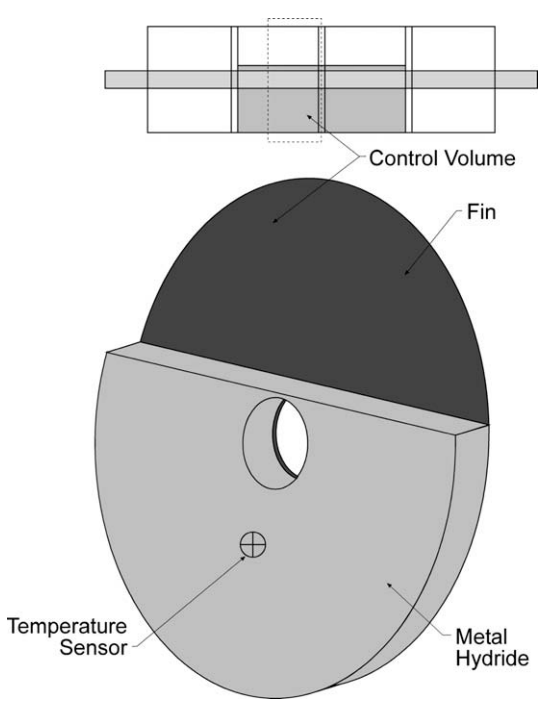

Fig. 6. Control volume used in the Fluent™ numerical model.

The thermal resistance due to the thickness of the coolant tube is represented as a wall conduction resistance in the simulations. The fin is made of copper, and the coolant tube is made of stainless steel. All other boundaries are assumed to be adiabatic, and end effects have been ignored. The temperature sensing point shown on Fig. 6 is located at the experimental probe position. Further, the initial temperature of the control volume is set at 5 °C to match the experimental conditions.

4. Results and discussion

The computational model was run initially to achieve grid and time step independence. The model converged with a time step of 0.5 s, a mesh of 184570 tetrahedral mesh volumes for the fin and 621143 tetrahedral mesh volumes for the metal hydride and with an approximate grid length of 0.02 in. (0.508 mm). After refining the mesh and the time step, the computational model was run by varying the different input parameters including the pressure function and the coolant flow rate. The temperature map of the control volume after 325 s of simulation for a 68 to 330 bar in 30 s pressurization profile is shown in Fig. 7.

4.1. Pressure function

In prior literature, different pressure-dependent functions, $f(P, P_{eq})$, have been suggested, including $\ln(P/P_{eq})$, (P/P_{eq}) and $(P/P_{eq})^2$. Prior literature suggests that the driving force is proportional to $\ln(P/P_{eq})$ when bulk diffusion limits the reaction rate [10,11] and is proportional to (P/P_{eq}) when surface transport is rate-limiting [3].

The Fluent™ model was run with three aforementioned pressure functions, keeping the other input parameters the same (pressurization from 68 to 330 bar in 30 s and coolant flow rate of 0.9 lpm, giving a heat transfer coefficient, h of 1100 W/m^{2}K). The metal hydride temperatures obtained are plotted in Fig. 8, along with the experimental metal hydride temperature profile at the same location and the experimental hydrogen gas temperature. Among the functions, $\ln(P/P_{eq})$ and (P/P_{eq}) produce results that are closer to the experimental metal hydride temperature profile than those obtained with $(P/P_{eq})^2$.

As shown in Fig. 8, some disparity exists between the experimental and numerical temperatures with a maximum difference of approximately 10 °C. This difference can be attributed to the absence of heat transfer between the gas and the composite metal hydride/hydrogen porous medium assumed in the model. Clearly, during pressurization ($t < 30$ s), the experimental hydrogen temperature in the pressure vessel is higher than the metal hydride temperature, indicating that the metal hydride is heated by the gas around it.

The kinetic parameters used in the model seem to be appropriate and cannot be more accurately estimated using the available model and experimental data. The slopes of the temperatures obtained with the model during the pressurization from 5 to 30 s are similar to those observed in the experimental data, indicating that the thermal capacitance used in the model simulates the experimental situation well.

The Fluent™ model was then run for three different pressure functions with conditions similar to test with pressurization profiles from 68 to 278 bar in 30 s and coolant flow rate of 3.8 lpm corresponding to a heat transfer coefficient, h of 7200 W/m^2-K. The metal hydride temperatures obtained are plotted in Fig. 9, along with the experimental metal hydride temperature profile at the same location and the experimental hydrogen gas temperature. Here again, the functions $\ln(P/P_{eq})$ and (P/P_{eq}) predict temperatures closer to the experimental data than the function $(P/P_{eq})^2$. The tem-

Table 1
Coolant flow rates with heat transfer coefficients.

Flow #	Flow rate (lpm)	Mass flow rate (g/s)	*Re*	*Nu*	*h* (W/m^2/K)	Correlation
1	0.38	0.006	800	8	900	Hausen
2	0.8	0.013	1700	12	1100	Hausen
3	3.8	0.06	8000	80	7200	Petukhov
4	9.5	0.16	20,000	180	17,000	Petukhov
5	19	0.32	40,000	340	30,000	Petukhov

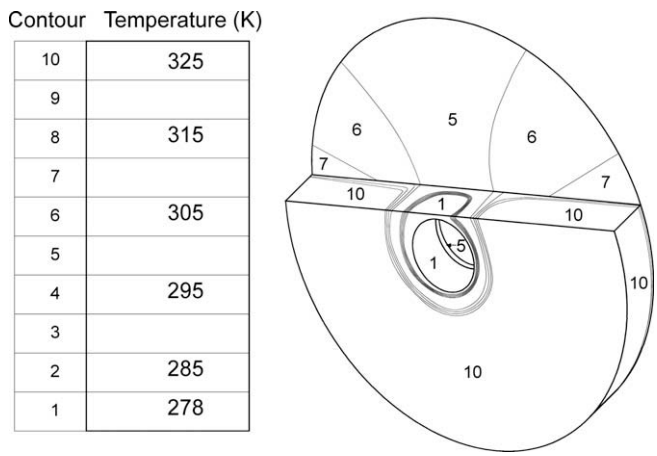

Fig. 7. Temperature map (degrees K) from a numerical simulation after 50 s.

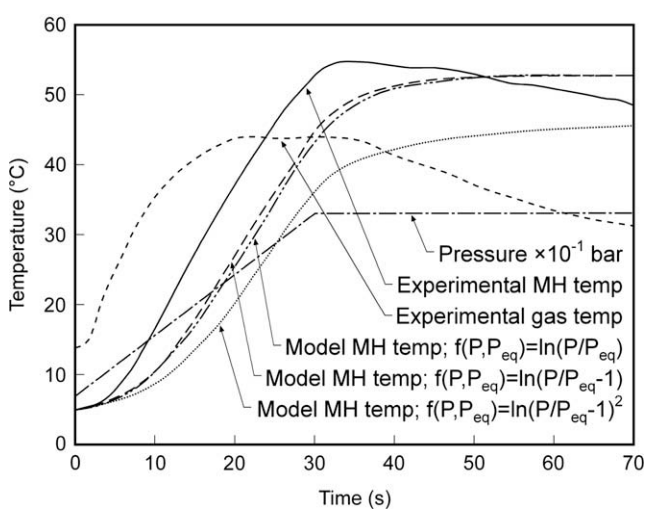

Fig. 8. Comparison of numerical results for different pressure functions with experimental data for the pressurization from 68 to 330 bar in 30 s and coolant flow of 0.9 lpm.

peratures obtained with the functions $\ln(P/P_{eq})$ and (P/P_{eq}) have a maximum temperature difference of 5 °C with the experimental metal hydride temperature during pressurization ($t < 30$ s). This deviation is attributed to the exchange of heat from the surrounding hotter hydrogen to the metal hydride powder.

In the experiments, the metal hydride cools after the pressurization ($t > 30$ s) due to heat loss to the surrounding hydrogen and conduction to the coolant tube and the pressure vessel. The model assumes adiabatic boundary conditions and therefore does not include heat losses to the hydrogen gas and the pressure vessel. Hence, the temperatures are higher in the model for $t > 30$ s.

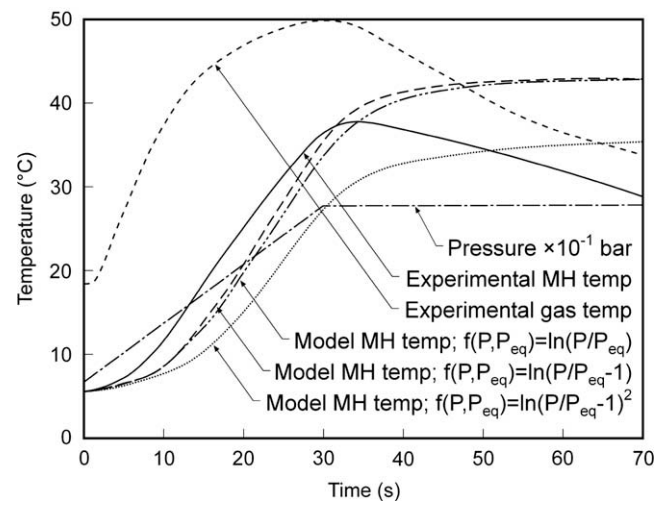

Fig. 9. Comparison of numerical results for different pressure functions with experimental data for the pressurization from 68 to 278 bar in 30 s and coolant flow of 3.8 lpm.

4.2. Reaction progress

The model was used to simulate a test condition for pressurization from 68 to 330 bar in 30 s with a coolant flow of 19 lpm ($h = 30{,}000$ W/m^2 K), and the results are compared with experimental data in Fig. 10.

The model predicts the temperatures of the metal hydride well during the pressurization time of 30 s. The cooling of the metal hydride ($t > 30$ s), however, is very different, as the model assumes adiabatic conditions on the boundary, while, in reality, heat is lost to the hydrogen and pressure vessel. Further, the model also does

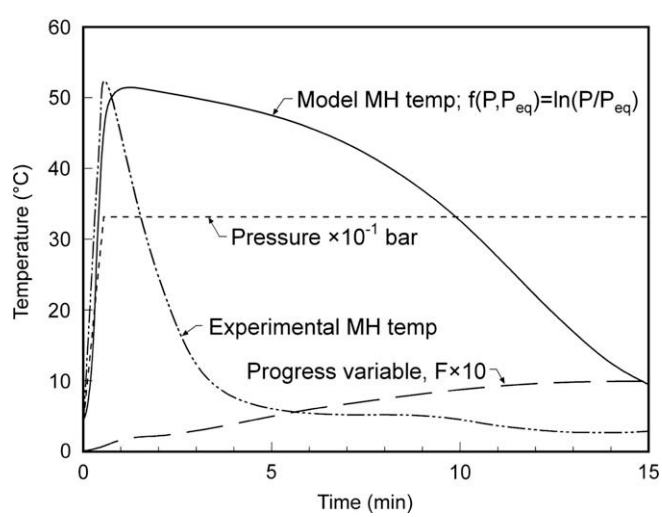

Fig. 10. Results for pressurization from 68 to 330 bar with coolant flow of 20 lpm.

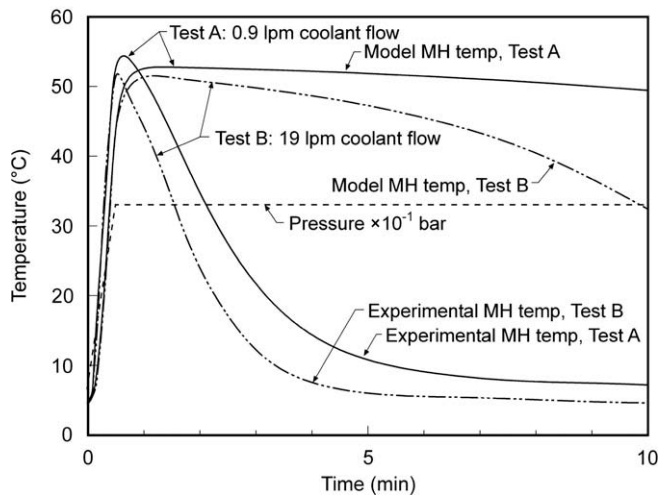

Fig. 11. Results with different coolant flow rates for a pressurization profile of 68–330 bar in 30 s.

not include the thermocouple probe which is a heat sink as well. The model can be improved by the addition of these effects.

4.3. Effect of coolant flow rate

Shown in Fig. 11 is a plot of experimental and computed metal hydride temperature profiles for two different coolant flow rates of 0.9 lpm (h = 1100 W/m^2-K) and 19 lpm (h = 30,000 W/m^2-K). Little difference exists in the temperatures in the initial period (t < 30 s) for both experimental and numerical cases. The maximum temperatures reached are lower for the higher coolant flow rate, as seen in experimental results.

5. Conclusions

Reversible, low-temperature metal hydrides represent a promising class of on-board hydrogen storage materials, in which heat and mass transfer play very important roles in both hydrogen absorption and desorption processes. Over the last two years, the Hydrogen Systems Lab, part of the Maurice Zucrow Laboratory at Purdue University, has been involved in testing hydrogen storage systems based on reversible, low-temperature metal hydrides. Safe operations at the Hydrogen Systems Lab have been proven at pressures up to 350 bar. Through careful planning and a close collaboration between researchers at the Purdue University Hydrogen Systems Lab and at General Motors, research culminated in the design and repeated safe testing of a practical high-pressure metal hydride storage system. The test article allowed for the characterization of the thermal behavior of $Ti_{1.1}MnCr$ during hydriding and dehydriding. Tests were conducted using this material by varying the pressurization profile and using different coolant flow rates. The hydriding process was modeled using a three-dimensional model in Fluent. While the model allows for accurate predictions of metal hydride temperature under different pressurization profiles and coolant flow rates, it fails to capture the temperature decay rates observed experimentally. This lack of agreement between experimental and computed temperature profiles clearly suggest that the model needs to take into account the mass of hydrogen gas in the pressure vessel as well as the combined thermal mass of the thermocouple probe and the containment vessel. Furthermore, the material properties used in the model, including the kinetic parameters and thermal properties, can be further refined to better simulate the experimental behavior, especially after pressurization. This additional study was not pursued with the existing experimental data due to the limited amount of metal hydride powder available for the tests and the relatively high amount of compression heating and convection heat losses to the hydrogen gas. Further, the modeling can be extended to predict the temperatures during desorption processes as well.

Acknowledgements

The authors are grateful to General Motors for their financial and technical support. The authors would also like to thank the students of the Hydrogen Systems Laboratory at Purdue University who aided in the overall progress of the work.

References

[1] A. Zuttel, Materials for hydrogen storage, Mater. Today 6 (9) (2003) 24–33.
[2] L.K. Heung, Using metal hydride to store hydrogen, DOE report, WSRC-MS-2003-00172, 2003.
[3] M.V.C. Sastri, B. Viswanathan, S. Murthy, Metal Hydrides, Narosa Publishing House, New Delhi, 1998 (Chapter 1).
[4] R. Gopal, S. Murthy, Studies on heat and mass transfer in metal hydride beds, In. J. Hydrogen Energy 20 (1995) 911–917.
[5] J.S. Zhang, T.S. Fisher, P.V. Ramachandran, J.P. Gore, I. Mudawar, A review of heat transfer issues in hydrogen storage technologies, ASME J. Heat Transfer 127 (12) (2005) 1391–1399.
[6] J.T. Koh, A.J. Goudy, P. Huang, G.A. Zhou, Comparison of the hydriding and dehydriding kinetics of $LaNi_5$ hydride, J. Less-Common Met. 153 (1) (1989) 89–100.
[7] Y. Kojima, Y. Kawai, S. Towata, T. Matsunaga, T. Shinozawa, M. Kimbara, Development of metal hydride with high dissociation pressure, J. Alloy Compd. 419 (1–2) (2006) 256–261.
[8] National Research Council, The Hydrogen Economy: Opportunities, Costs, Barriers, and R&D Needs, The National Academies Press, Washington, DC, 2004.
[9] Y. Zheng, V. Velagapudi, T. Pourpoint, T.S. Fisher, I. Mudawar, J.P,.Gore, Thermal management analysis of on-board high-pressure metal hydride systems, in: Proceedings of ASME International Mechanical Engineering Congress and Exposition, IMECE2006-14080, 2006.
[10] P.D. Goodell, P.S. Rudman, Hydriding and dehydriding rates of the $LaNi_5$–H system, J. Less-Common Met. 89 (1) (1983) 117–125.
[11] M. Miyamoto, K. Yamaji, Y. Nakata, Reaction-kinetics of $LaNi_5$, J. Less-Common Met. 89 (1) (1983) 111–116.
[12] S.B. Nasrallah, A. Jemni, Heat and mass transfer models in metal-hydrogen reactor, Int. J. Hydrogen Energy 22 (1) (1997) 67–76.
[13] P.S. Rudman, Hydriding and dehydriding kinetics, J. Less-Common Met. 89 (1) (1983) 93–110.
[14] G.A. Sandrock, A panoramic overview of hydrogen storage alloys from a gas reaction point of view, J. Alloy Compd. 295 (1999) 877–888.
[15] R.B. Bird, W.E. Stewart, E.N. Lightfoot, Transport Phenomena, John Wiley & Sons, 1960 (Chapter 10).
[16] G. Sandrock, S. Suda, L. Schlapbach, Hydrogen in Intermetallic Compounds II: Surface and Dynamic Properties, Applications, Springer-Verlag, Berlin, 1992 (Chapter 5).
[17] D. Ohlendorf, H.E. Flotow, Heat-capacities and thermodynamic functions of $LaNi_5$, $LaNi_5H_{0.36}$ and $LaNi_5H_{6.39}$ from 5 to 300 K, J. Less-Common Met. 73 (1) (1980) 25–32.
[18] J. Kapischke, J. Hapke, Measurement of the effective thermal-conductivity of a metal hydride bed with chemical-reaction, Exp. Therm. Fluid Sci. 9 (3) (1994) 337–344.
[19] S. Suda, N. Kobayashi, K. Yoshida, Reaction-kinetics of metal-hydrides and their mixtures, J. Less-Common Met. 73 (1) (1980) 119–126.
[20] F.P. Incropera, D.P. DeWitt, Fundamentals of Heat and Mass Transfer, John Wiley & Sons, 1996 (Chapter 8).